Check for updates

Self-Powered Intelligent Voice Navigation Tactile Pavement Based on High-Output Hybrid Nanogenerator

Dongjie Jiang, Minxing Du, Xuecheng Qu, Yansong Gai, Wei Sun, Jiangtao Xue, Yusheng Li, Zhou Li,* and Zhong Lin Wang*

Improving the safety and usability of the blind movement is of great significance. The blind navigation system has always been the focus of attention. However, achieving an unconscious interaction and long-term operation with high navigation accuracy is an urgent challenge. In this study, a distributed self-powered intelligent voice navigation tactile pavement (SVP) based on a hybrid nanogenerator for blind navigation is reported. More than 4-s effective output time is achieved under a single instantaneous pressure to the hybrid nanogenerator. The system is integrated with an inertial storage hybrid nanogenerator (ISNG), RF transmitter module, and voice broadcast module. It has the advantages of outstanding navigation accuracy, fatigue resistance (16 000 cycles), temperature stability (–50 to 50 °C), no required operation, and easy fabrication. The SVP may solve the difficulties of GPS navigation delay and lack of map information and realize the accurate identification and feedback of key locations, providing an effective and unconscious interaction navigation strategy for the blind. Integrating the hybrid nanogenerator under the road can provide an energy supply for the construction of the Internet of Things and smart city in the future.

1. Introduction

According to the World Health Organization, there are about 285 million people have visual impairment or blindness in the world. Of these people, around 39 million are blind at least, and it is expected that the population with visual impairment will continue to increase in the next few decades.[1] Blind people are facing many difficulties every day due to their inability to detect objects. In particular, imperfect barrier-free facilities make it more difficult for the blind to walk. Therefore, seeking a safe and effective navigation strategy is what the blind expects.[2]

With the development of the Internet of Things (IoT), the intelligence of navigation systems has been continuously improved, which has become a necessary tool for people's daily life.[3] However, visual impairment makes it impossible for the blind to easily use the common intelligent navigation equipment to ensure convenient travel. They need a specialized device that is designed for the blind.[4] To most of the existing equipment, the navigation function is based on the digital commercial Global Position System (GPS), which is not suitable for the area with no GPS map. And the positioning is not accurate enough due to the location information refresh delay and hardware facility.[5] Moreover, the complicated operation process and

D. J. Jiang, M. X. Du, X. C. Qu, Y. S. Gai, W. Sun, J. T. Xue, Z. Li
CAS Center for Excellence in Nanoscience
Beijing Key Laboratory of Micro-nano Energy and Sensor
Beijing Institute of Nanoenergy and Nanosystems
Chinese Academy of Sciences
Beijing 101400, China
E-mail: zli@binn.cas.cn

D. J. Jiang, X. C. Qu, W. Sun, J. T. Xue
School of Nanoscience and Technology
University of Chinese Academy of Sciences
Beijing 100049, China

M. X. Du
School of Resources
Environment and Materials
Guangxi University
Nanning 530004, China

Y. S. Gai
School of Chemistry and Chemical Engineering
Guangxi University
Nanning 530004, China

The ORCID identification number(s) for the author(s) of this article can be found under https://doi.org/10.1002/admt.202200270.

DOI: 10.1002/admt.202200270

Y. S. Li
Department of Orthopedics
Xiangya Hospital
Central South University
Changsha 410008, China
E-mail: liyusheng@csu.edu.cn

Y. S. Li
National Clinical Research Center for Geriatric Disorders
Xiangya Hospital
Central South University
Hunan, Changsha 410008, China

Z. Li
Center on Nanoenergy Research
School of Physical Science and Technology
Guangxi University
Nanning 530004, China

Z. Li
Institute for Stem Cell and Regeneration
Chinese Academy of Sciences
Beijing 100101, China

Z. L. Wang
School of Materials Science and Engineering
Georgia Institute of Technology
Atlanta, GA 30332, USA

© 2022 Wiley-VCH GmbH

noninteractive user experience are unfriendly to the blind. In most cases, the walking routes are complex and diverse, not keeping a single straight line. Therefore, accurate identification and feedback of key locations are crucial for blind navigation. Such as the crossroads and destination. When the GPS map is lost or not detailed enough, the only option is to navigate in the planned orbit. Erroneous identification of key locations may be fatal for the visually impaired.[6] By constructing the distributed intelligent voice navigation network in the city to feedback the key location information to the blind precisely, we can prevent these problems and realize barrier-free and safe travel for the blind.

However, the power supply of a large number of distributed navigation devices is a huge challenge, which brings great difficulties to the construction of Internet of Things. Fortunately, energy harvesting technologies and equipment have proven their unique ability to power distributed electronics, such as electromagnetic generator (EMG),[7] triboelectric nanogenerator (TENG),[8] piezoelectric nanogenerator (PENG),[9] and biofuel cell.[10] These technologies can convert the mechanical energy of human movement or the biomass energy of the human body into electricity to power wearable and portable electronics. As an efficient and environment-friendly mechanical energy harvesting technology, TENG can generate a voltage output of tens to hundreds of volts when the current output is dozens of microamps. TENG has been rapidly developed due to the simple manufacturing processes, a wide range of material choices, and high output voltage.[11] Electromagnetic generators can also convert biomechanical energy into electricity based on electromagnetic induction.[12] The size of the permanent magnet and the turns of the coil will directly influence the output. In recent research, the hybrid utilization of these energy harvesting technologies has shown encouraging prospects for the Internet of things.[13] However, biomechanical motion is always low-frequency and discontinuous, which makes it difficult for the harvester to convert efficiently to drive the high-power electronics.[14]

Here, we present a self-powered intelligent voice navigation tactile pavement based on an inertia storage hybrid nanogenerator (ISNG) that is consisted of triboelectric nanogenerator (TENG) and electromagnetic generator (EMG). Under a single instantaneous external force, ISNG can generate electricity continuously for about 4 seconds. TENG can produce a maximum open-circuit voltage of 25 V and a short-circuit current of 0.6 μA. EMG can produce a maximum open-circuit voltage of 5 V and a short-circuit current of 3.5 mA. ISNG has the ability to power a variety of electronic devices, such as LED, hygrometer, and mobile smartphone. Finally, we have built a self-powered intelligent voice navigation tactile pavement (SVP) composed of ISNG, RF transmitter module, and voice broadcast module. Imitating the design of tactile pavement, ISNG is placed under the pavement. When the blind steps on the convex structure of the tactile pavement, the ISNG at the bottom can convert the biomechanical energy of the human motion into electrical energy that can power the RF module for launching an RF signal. After receiving the RF signal, the voice broadcast module nearby the key location can automatically broadcast the information. We have presented that SVP can guide the blind walking from the bus stop through the intersection and finally reach the supermarket. These convincingly demonstrate that SVP can improve navigation accuracy and be utilized as a part of the blind navigation system to enhance safety and usability for blind movement.

2. Results and Discussion

2.1. Self-Powered Intelligent Voice Navigation Tactile Pavement

Many regular permutation protrusions are fixed on the surface of the tactile pavement, and the height of each protrusion is about 5 mm. The blind can use their feet to sense the protrusion and correct the walking direction. There are three common protrusions: spherical, square, and cylindrical. While preserving this structure, we have designed a self-powered intelligent voice navigation tactile pavement (SVP) (**Figure 1**a). The system includes ISNG and RF transmitting modules fixed under the protrusion and a voice broadcast module distributed on the road (Figure 1b). The screw rod of ISNG is distributed in the middle of these protrusions, which work for transmitting the kinetic energy of the human motion to ISNG (Figure 1a).

When the foot stamp on the protrusion, the middle protrusion will drop to be flush with the ground leading to the screw rod being pressed down to drive the generator rotation. Because of the existence of other permutation protrusions, there is no discomfort during walking on the SVP. The electricity generated by the ISNG drives the RF module to launch a wireless signal to the voice broadcast module on the road. After receiving the RF signal, the voice broadcast module will respond and automatically broadcast nearby location information, such as supermarkets, bus stops, and crossroads. The blind can get feedback on their current location through voice broadcasting. Compared with the common GPS navigation system, the self-powered intelligent voice navigation tactile pavement can instantaneously and accurately broadcast the key location information, avoiding the travel disturbance of the blind caused by the GPS network refresh delay and map information error.

2.2. Structural Design of ISNG

ISNG consists of four parts: inertial storage structure, power generation structure, elastic recovery structure, and support structure (Figure 1d). The inertial storage structure and elastic recovery structure constitute the transmission structure of ISNG, which can convert the linear motion into horizontal rotational motion (Figure 1e). By the unique mechanical transmission structure, ISNG can convert the single instantaneous pressure into continuous rotational motion over 4 s. After the external force is removed, the rotation of the rotor is not hindered. Until the next external force is applied to the ISNG, the rotation speed of the rotor will be accelerated (Video S1, Supporting Information).

The power generation structure is composed of TENG and EMG. Both of them are dependent on horizontal rotary motion (Figure 1c). As the rotator, the 5 mm thick acrylic disc prepared by laser cutting is fixed with the transmission structure. Eight magnets are evenly embedded at the edge of the disc, and four

 © 2022 Wiley-VCH GmbH

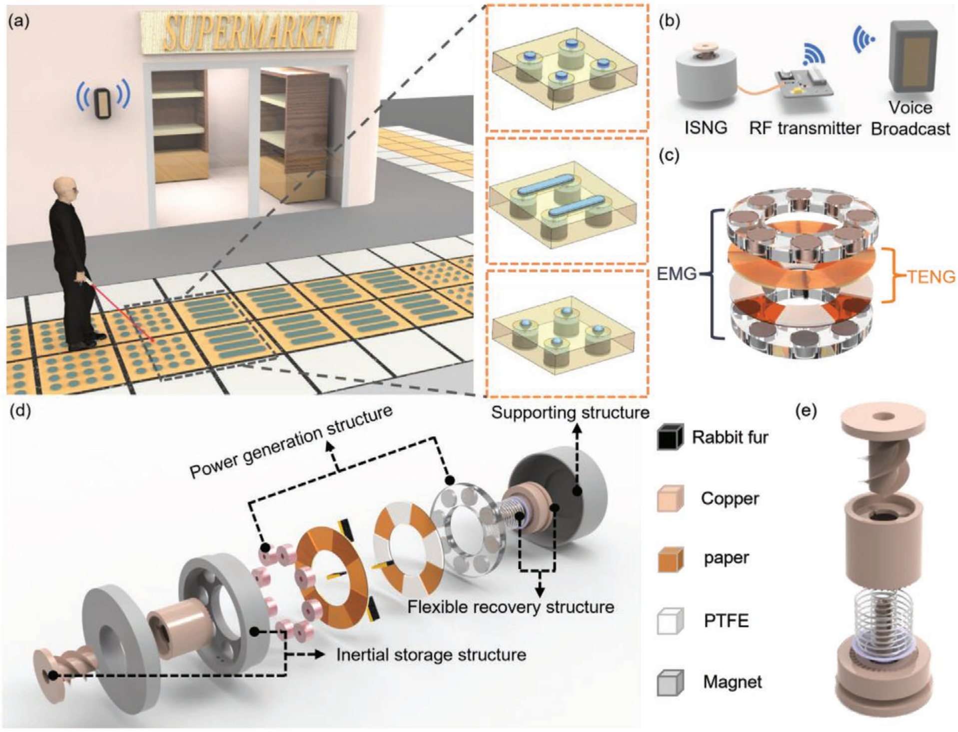

Figure 1. a) Concept diagram of SVP. b) Composition diagram of SVP. c) Power generation structure of ISNG. d) The explosive diagram of ISNG. e) Mechanical transmission structure of ISNG.

fan-shaped PTFE are evenly attached to the surface of the disc. As the stator, eight series connection copper coils are evenly embedded on the intermediate shell prepared by 3D printing. The positions of the eight copper coils are opposite to the eight magnets (Figure S1, Supporting Information). The annular interdigital copper electrode adheres to the lower surface of the intermediate housing opposite to PTFE. Four pieces of rabbit fur are pasted vertically in the gap of the interdigital electrode. And the whole device is wrapped with PTFE film to improve its waterproof performance.

2.3. Working Principle of ISNG

We have proposed the working principle of ISNG in one cycle (**Figure 2**a). The mechanism of TENG is based on the triboelectric and electrostatic induction effect of two materials with different electronegativity during the relative movement (Figure 2b). The rotor of the transmission structure drives the acrylic disc to rotate. In the initial state, PTFE is located in the gap position of the interdigital electrode, and then PTFE rotates to the E2 position. Due to the abundant negative charge on the surface of the corona discharge treated PTFE, an equal amount of positive charge is induced on the E2 electrode surface. In the external circuit, the positive charge flows from E1 to E2. When PTFE rotates from the E2 position to the gap position of the interdigital electrode, the positive charge induced on the surface of the E2 electrode decreases gradually because the overlapping area between PTFE and E2 electrode decreases gradually. In the external circuit, the positive charge flows from E2 to E1. Rabbit fur here plays a role in supplementing charge for PTFE surface.

We use a DC motor to drive the friction generator at a constant speed of 350 rpm. In this condition, TENG can generate an open-circuit voltage of 25 V and a short-circuit current of 0.5 μA (Figure 2d). The peak values of open-circuit voltage remain stable with the gradual decrease in the rotational speed, while the short-circuit current gradually decreases. That is because the rotational speed has no influence on the transferred charge density under a constant contact area. And a higher rotational speed results in a faster charge transfer rate. The open-circuit voltage and the short-circuit current can be derived by the equation as follows

$$I_{SC} = \frac{dQ}{dt} \tag{1}$$

$$V_{OC} = \frac{Q}{C} \tag{2}$$

Here, Q is the transferred charge, C is the capacitance, t refers to time. It can be seen that the current values are determined by the transferred charge and time. Hence, there is no correlation between the open-circuit voltage of TENG and rotating speed. The short-circuit current has a linear relation with rotational speed.

The rotor of the transmission structure drives the disk with magnets embedded at the edge to rotate. The copper coil in the middle shell is affected by the changing magnetic field, and the induced current is generated in the coil. At a constant speed of 350 rpm, the electromagnetic generator can generate an open circuit voltage of 4 V and a short circuit current of 3 mA (Figure 2e). The open-circuit voltage and the short circuit current can be derived by the equation as follow:

© 2022 Wiley-VCH GmbH

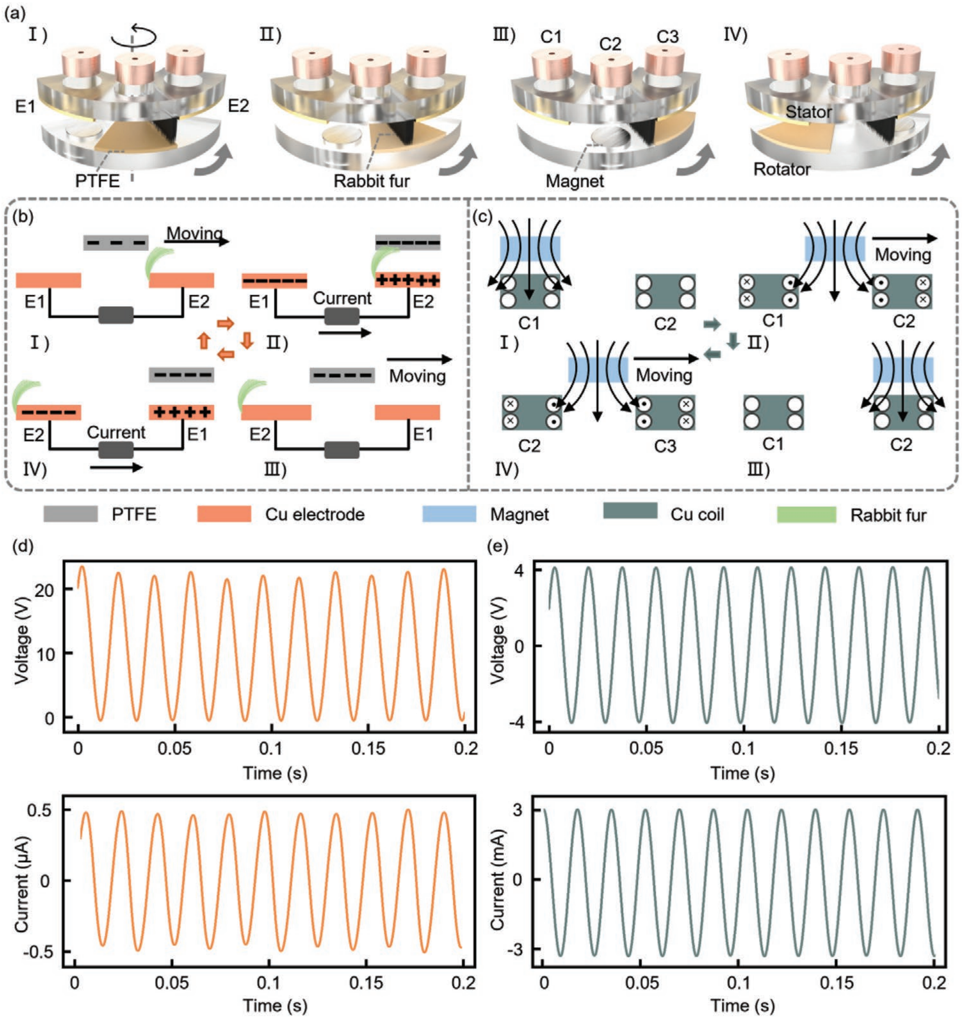

Figure 2. a) Schematic diagram of ISNG in a complete cycle. b) Schematic diagram of the working mechanism of TENG. c) Schematic diagram of the working principle of EMG. The short-circuit current and open-circuit voltage of d)TENG and e) EMG at a constant speed (350 rpm).

$$V_{OC} = n\frac{d\Phi}{dt} \tag{3}$$

$$I_{SC} = n\frac{d\Phi}{Rdt} \tag{4}$$

Here, V_{OC} is the open-circuit voltage, I_{SC} is the short-circuit current, Φ refers to magnetic flux, R is source impedance, n refers to the number of turns of the coil, and t refers to time. Thus, the open-circuit voltage and the short-circuit current of EMG have a linear relationship with rotational speed.

2.4. Electrical Characterization of ISNG

We use a vertical linear motor to simulate the movement of human feet lifting and falling, as shown in **Figure 3**a. Under the pressure condition of 8 m s^{-2} acceleration and 9 mm vertical displacement, TENG can generate a maximum open-circuit voltage of 25 V, and a maximum short-circuit current of 0.6 µA (Figure 3b,c). EMG can generate a maximum open-circuit voltage of 5 V, and a maximum short-circuit current of 3.5 mA (Figure 3e,f). To investigate the impedances of the TENG and EMG unit of the ISNG, the output current and voltage are measured under the different loading resistances. The output voltage of TENG and EMG increases with the increase of load, the output current decreases with the increase of load, and the output power increases at first and then decreases with the increase of load. Under the load of 60 MΩ, the maximum output power of TENG is 2.7 µW (Figure 3d). Under the load of 1800 Ω, EMG can obtain a maximum output power of 4.7 mW (Figure 3g). The continuous and stable output performance of ISNG at the loading frequency of 1Hz shows its potential as a wearable power supply unit (Figure 3h,i). In order to explore the durability of ISNG, we have done 16 000 loading tests under low frequency (0.35 Hz). After the fatigue tests, ISNG still maintains stable output performance, which shows that ISNG has the ability of long-term service (Figure 3j). Moreover, the waterproof performance of the device still shows an excellent result after the durability test (Figure S4, Supporting Information).

The output performance of the ISNG depends on the maximum speed of the internal rotor. The maximum speed of the

 © 2022 Wiley-VCH GmbH

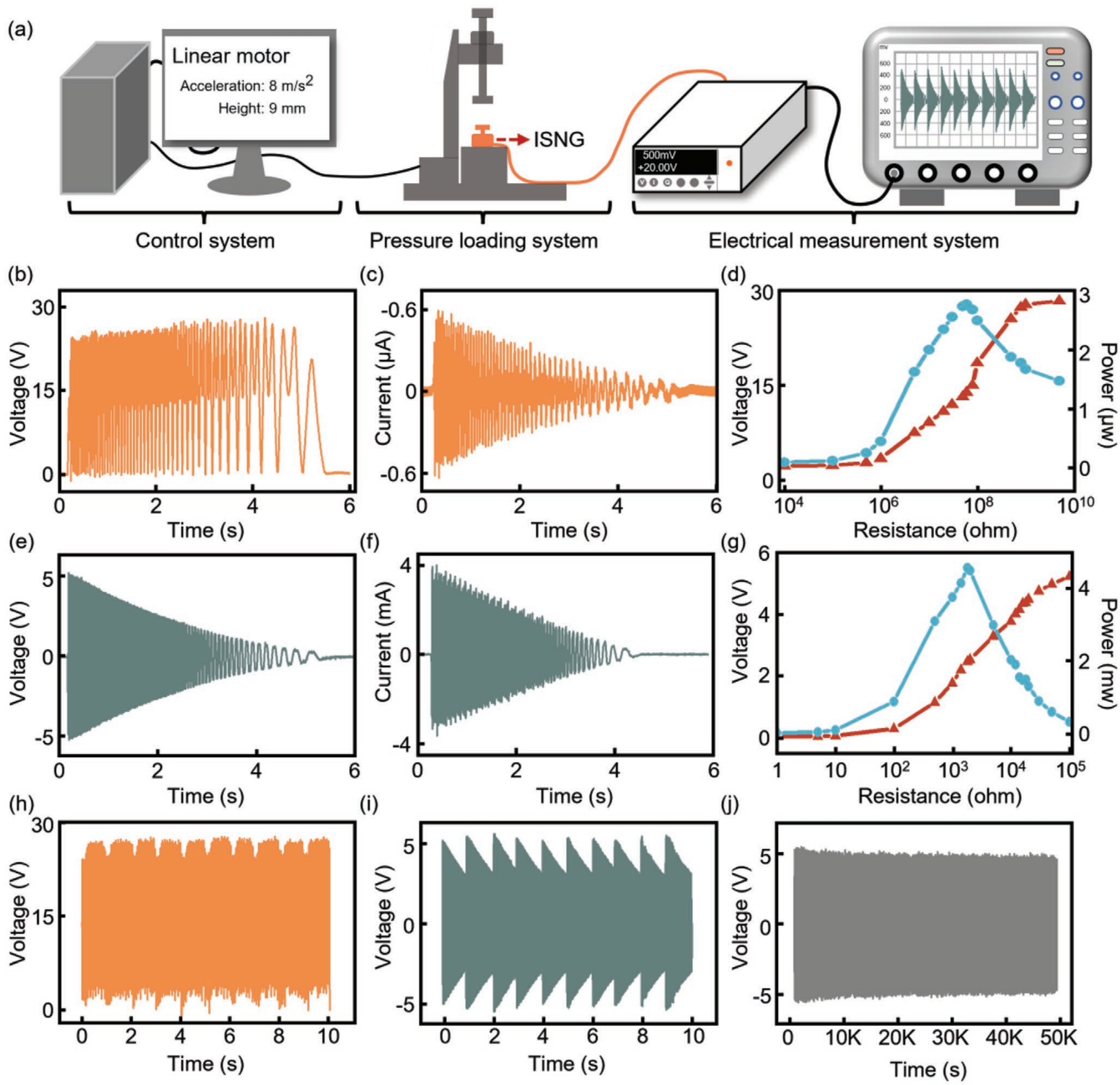

Figure 3. a) Schematic diagram of a system to simulate pressure changes. b) Open-circuit voltage and c) short-circuit current of TENG under a single load. d) The relationships between the output voltage/power and the loading resistance of TENG. e) Open-circuit voltage and f) short-circuit current of EMG under a single load. g) The relationships between the output voltage/power and the loading resistance of EMG. The continuous output voltage of h) TENG and i) EMG at a 1-Hz frequency load. j) Fatigue test of ISNG.

rotor is positively correlated with the downward speed when the vertical screw rod to the lowest point. Therefore, we explored the influence of the vertical downward acceleration and downward displacement of the screw rod on the output performance of ISNG. First, press the screw rod with an acceleration of 10 m s^{-2}. When the downward height of the screw rod is reduced from 9 to 5 mm, the maximum output voltage of EMG is reduced from 6 to 4 V, the maximum output voltage of TENG remains unchanged, and the continuous output time of both is reduced from 6 to 4 s. Second, the vertical descending displacement is maintained at 9 mm. When the acceleration of the screw rod is reduced from 10 to 2 m s^{-2}, the maximum output voltage of EMG is reduced from 6 to 3 V, and the maximum output voltage of TENG remains unchanged. The continuous output time of both is reduced from 6 to 3 s (**Figure 4**a,b; Figure S5, Supporting Information). At the same time, we measured and fitted the output values of ISNG under different accelerations and heights. It was found that the maximum output peak value and output time of ISNG increased with the increase with the acceleration and vertical downward displacement of the external force (Figure 4c,d).

 © 2022 Wiley-VCH GmbH

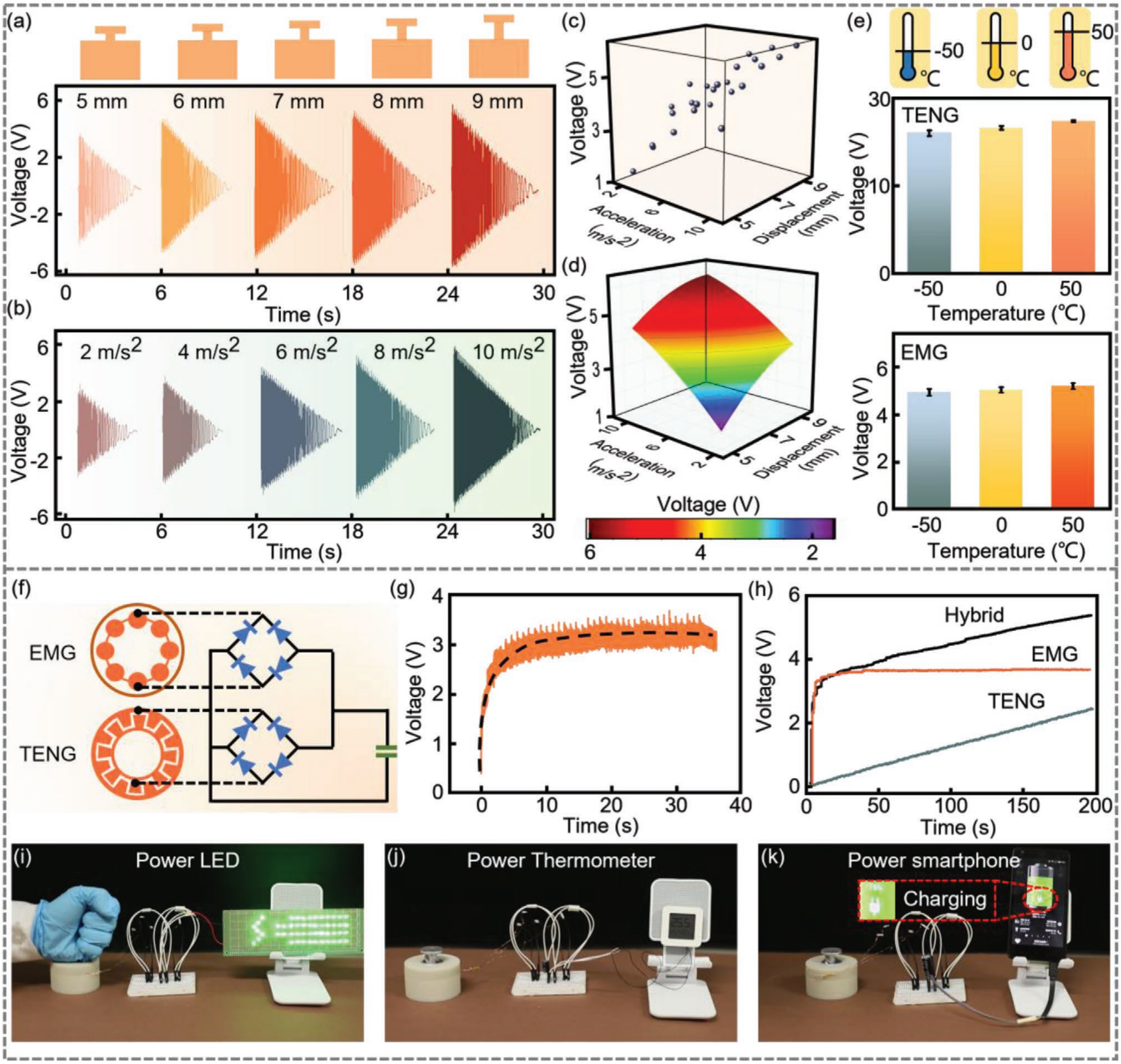

Figure 4. a) Open-circuit voltage of EMG at different pressing vertical downward displacements under 10 m s^{-2} pressure acceleration. b) Open-circuit voltage of EMG at different pressing accelerations at 9 mm downward displacement. c) Scatter diagram and d) nonlinear fitting diagram of EMG's open-circuit voltage under different pressing displacements and pressing acceleration. e) Open-circuit voltage of EMG and TENG at different temperatures ($n = 3$). f) Charging circuit diagram of ISNG. g) Lithium-ion battery (≈0.8 mAh) charge curve of ISNG. h) Capacitor (47 µF) charge curve of each part and ISNG. Application as the universal power source for i) LED, j) thermometer, and k) smartphone.

Since the ISNG will be utilized in an open-air environment, we use mechanically and chemically stable PTFE film for packaging the ISNG as a whole to avoid the impact of air humidity on its output. We successfully powered the LED by ISNG underwater (Video S2, Supporting Information). Because the environment temperature varies greatly throughout the four seasons, we measured the output performance of the ISNG at different temperatures. First, we have measured its output performance at room temperature. Second, we placed it in an electric constant temperature drying oven at 50 °C for 5 h, and then took it out and measured its short-circuit current and open-circuit voltage immediately. Finally, we put ISNG into the refrigerator at −50 °C for 5 h, and then tested its output performance. After treatment at different temperatures, it can be found that the output of TENG and EMG fluctuates little within the ambient temperature range, proving the ability of outdoor service (Figure 4e).

A battery and capacitor are used as the energy storage unit to drive the electronics stably and continuously in this research. The two power generation types of ISNG are connected in parallel (Figure 4f). ISNG can instantly charge a small battery of 0.8 mAh to 3 V under the conditions of 6 m s^{-2} acceleration and

© 2022 Wiley-VCH GmbH

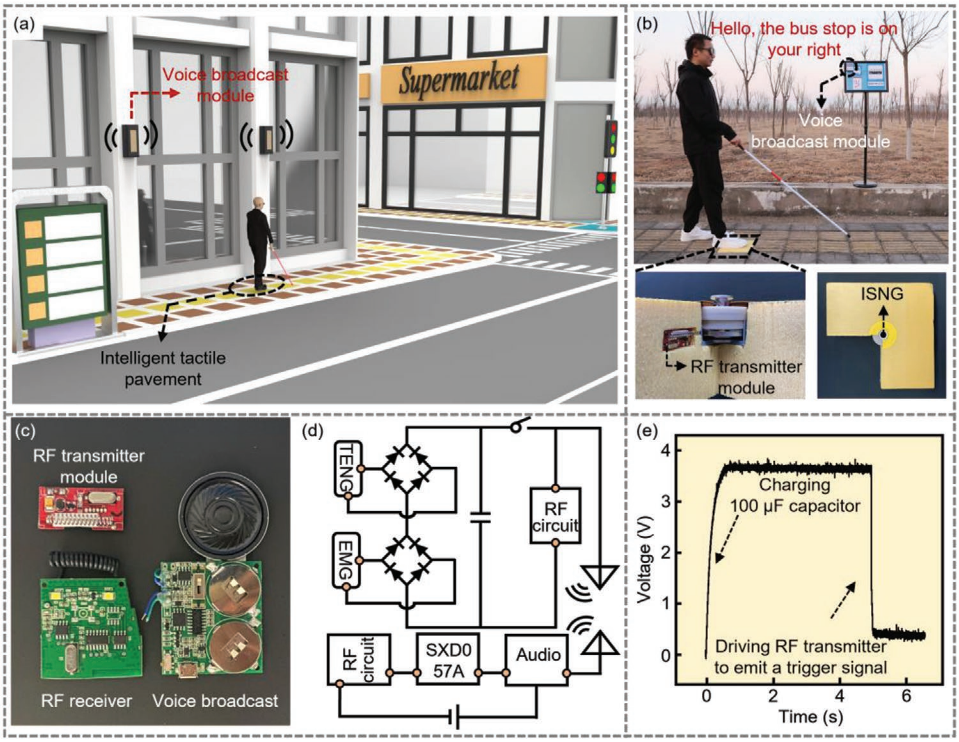

Figure 5. a) Designed diagram and b) picture of SVP. c) Picture of integrated RF transmitter module and voice broadcast module of SVP. d) Simplified circuit diagram of SVP. e) Voltage changes of a 100 μF capacitor charged by ISNG and used to power the RF transmitter module to emit a trigger signal.

9 mm stamp vertical displacement (Figure 4g). When ISNG is stamped by the foot and the vertical displacement is 5 mm, the electric energy generated by the ISNG can charge the capacitor (47 μF) over 3 V instantaneously (Figure 4h). Benefitting from TENG's high output voltage characteristic, the ISNG can still charge the capacitor to 5 V, which is beyond the output voltage of EMG on this condition (Figure 4h). EMG and TENG parallel compound strategy solves the defects of slow charging of TENG and a low charging voltage of EMG and realizes complementary advantages. ISNG can serve as a power supply unit for portable electronic equipment and supply power to different electronic equipment. A single load can drive the LED light to light for 4 s and the thermometer and hygrometer to work for 30 s. The continuous load can provide energy for mobile phone (Figure 4i–k; Video S3, Supporting Information). These applications show the potential of ISNG to be used as an outstanding biomechanical energy harvester for self-powered distributed electronics.

2.5. Application of ISNG in Blind Navigation

By combining ISNG with tactile pavement, we design a self-powered intelligent voice navigation tactile pavement (SVP) (**Figure 5**a). The system consists of three parts: ISNG and RF transmitter modules are located below the tactile pavement, and the voice broadcast module is located adjacent to the key navigation location (Figure 5b). The ISNG is placed under the tactile pavement and protrudes 5 mm from the pavement to imitate the protruding structure of the tactile pavement.

When the foot stamp on the protrusion of the ISNG, it can instantly charge 100 μF capacitors to 3.7 V after rectification, which can drive the ultra-low power consumption RF module and communicate with the RF receiver at the working frequency of 433.92 MHz (Figure 5c,d). After being processed by the microcontroller unit (MCU), the low-level signal was generated to trigger the MCU of the voice broadcast module. Then the paired voice broadcast module will instantaneously emit the voice prompt about location information. such as bus stops, life supermarkets, and intersections (Figure 5e). As shown in Video S4, Supporting Information, SVP can guide the blind walking from the bus stop through the intersection to the supermarket by voice feedback. SVP can eliminate the problem of GPS navigation delay or incomplete map information and provides convenience and safety for blind walking.

3. Conclusions

In summary, we have proposed a self-powered intelligent fixed-point voice navigation tactile pavement (SVP) driven by an inertial storage hybrid nanogenerator (ISNG) which is based on the triboelectric nanogenerator (TENG) and electromagnetic generator (EMG). ISNG imitates the convex structure of the tactile pavement, which can efficiently convert the kinetic energy of the human walking into electricity. When the ISNG is pressed under an instantaneous external force, it can generate electricity continuously over 4 s. The TENG can produce a maximum open-circuit voltage of 25 V and a maximum short-circuit current of 0.6 μA. The EMG can produce a maximum open-circuit voltage of 5 V and a maximum short-circuit current of 3.5 mA. Driven by foot, ISNG can power the RF transmitter module to send the key location information to the adjacent voice broadcast module. This distributed self-powered fixed-point voice navigation system may solve the problem of blind walking caused by GPS navigation refresh delay and lack of map information. The navigation accuracy can be improved by SVP to enhance the safety and usability of blind movement. At the same time, the distributed efficient power generation device below the road provides an energy supply for the construction of the intelligent city and the Internet of Things.

4. Experimental Section

Fabrication of Transmission and Support Structure: The material utilized in these structures was 3D printed polyamide 12 with 30% glass bead filler, which had excellent temperature resistance, dimensional stability, and toughness. The transmission structure was mainly composed of two groups of mechanical structures: a vertical reciprocating structure composed of a screw rod, internal thread sleeve and spring, and the other was a horizontal rotating structure composed of an internal thread sleeve, rotor, and support seat. When the screw rod moved downward, the surface friction of the screw cap limited its freedom of horizontal rotation, and the screw rod could only maintain vertical movement. Due to the small friction between the screw rod and the internal thread sleeve, when subjected to the vertical force of the screw rod thread, the internal thread sleeve produced two movement modes of horizontal rotation and vertical movement at the same time. The thin internal spring played the role of springing the screw rod, and the external thick spring suspended the internal thread sleeve. There were many serrations at the bottom edge of the internal thread sleeve and serrated indentations at the top of the rotor. When the internal thread sleeve moved downward, the serrations meshed with cogs, and the horizontal rotary motion drove the rotor to rotate.

Fabrication of EMG Part of ISNG: An acrylic annular disc with an outer diameter of 5 cm and an inner diameter of 2 cm was prepared by laser cutting. Eight through holes with a diameter of 1 cm were evenly cut at the edge of the annular disc to place the magnet. The annular disc was equipped with magnets and the rotor of the bottom of the transmission structure adopted an interference fit. 3D printing technology was used to prepare a shell for fixing and supporting the transmission structure. The shell was divided into three parts: top cover, middle, and bottom support. Eight through holes with a diameter of 1 cm were distributed on the edge of the middle shell for placing copper coils. When the transmission structure was pressed, the bottom rotor drove the acrylic annular disc to rotate. The copper coil in the middle shell was affected by the changing magnetic field to produce an induced current.

Fabrication of TENG Part of ISNG: The TENG was composed of three parts: charge resident layer (PTFE), inductive interdigital electrode, and charge supplement material (rabbit fur). Four fan-shaped PTFE were uniformly pasted on the upper surface of the annular acrylic disc prepared by laser cutting, and the inductive interdigital electrode was pasted on the lower surface of the middle shell of 3D printing. To further promote the output performance of ISNG, the corona discharge method was used to modify the PTFE surface to achieve a higher surface charge density.[15] Four pieces of rabbit fur were vertically pasted on the lower surface of the middle shell of 3D printing and distributed in the gap between the inner and outer ring of interdigital electrodes. When the transmission structure was pressed, the annular disc drove the PTFE on the surface to rotate. In the process of PTFE rotation, it constantly rubbed with the rabbit fur contact to accumulate charge. The interdigital electrode was affected by electrostatic induction, and the induced current was generated in the circuit.[16]

Characterization of ISNG: The electrical output performance of ISNG was measured by the electrometer (Keithley 6517B) and the oscilloscope (LeCroy HDO6104). The linear motor (LinMot E1100) was used to provide a periodic vertical external force applied to the ISNG.

Statistical Analysis: All results were performed with the sample size of $n = 3$. The statistics were expressed as the mean values ± SD (standard deviation). Origin 8.0 was used for statistical analysis.

Supporting Information

Supporting Information is available from the Wiley Online Library or from the author.

Acknowledgements

D.J., M.D., and X.Q. contributed equally to this work. The authors are grateful to Dr. Yang Zou, Dr. Lin Gao, and other laboratory members for their cooperation in this study. This study was supported by the National Natural Science Foundation of China (61875015, T2125003), the Strategic Priority Research Program of the Chinese Academy of Sciences (XDA16021101), the Beijing Natural Science Foundation (JQ20038, L212010).

Conflict of Interest

The authors declare no conflict of interest.

Data Availability Statement

The data that support the findings of this study are available from the corresponding author upon reasonable request.

Keywords

blind navigation, distributed devices, hybrid nanogenerator, self-powered electronics

Received: February 18, 2022
Revised: May 6, 2022
Published online:

[1] a) S. Khan, S. Nazir, H. U. Khan, *IEEE Access* **2021**, *9*, 26712; b) H. Fernandes, P. Costa, V. Filipe, H. Paredes, J. Barroso, Universal Access in the Information Society **2019**, *18*, 155.
[2] a) M. M. Islam, M. Sheikh Sadi, K. Z. Zamli, M. M. Ahmed, *IEEE Sens. J.* **2019**, *19*, 2814; b) Q. Shi, Z. Zhang, T. He, Z. Sun, B. Wang, Y. Feng, X. Shan, B. Salam, C. Lee, *Nat. Commun.* **2020**, *11*, 4609.
[3] a) L. Cao, X. L. Huang, *Adv. Mater. Res.* **2012**, *433*, 4184; b) R. Ivanov, *J. Network Comput. Appl.* **2012**, *35*, 1559; c) X. Li, M. Ge, X. Dai, X. Ren, M. Fritsche, J. Wickert, H. Schuh, *J. Geodesy* **2015**, *89*, 607.
[4] a) R. Velázquez, E. Pissaloux, P. Rodrigo, M. Carrasco, N. Giannoccaro, A. Lay-Ekuakille, *Appl. Sci.* **2018**, *8*, 578; b) A. Mishra, R. Mathew, in *Proceeding of the International Conference on Computer Networks, Big Data and IoT (ICCBI –2018)*, Springer, New York **2020**, p. 204.
[5] S. Godha, M. E. Cannon, *GPS Solutions* **2007**, *11*, 193.
[6] a) S. Real, A. Araujo, *Sensors (Basel)* **2019**, *19*, 3404; b) F. E. El-Taher, A. Taha, J. Courtney, S. McKeever, *Sensors (Basel)* **2021**, *21*, 3103.

 © 2022 Wiley-VCH GmbH

[7] a) L. C. Rome, L. Flynn, E. M. Goldman, T. D. Yoo, *Science* **2005**, *309*, 1725; b) P. Maharjan, T. Bhatta, M. Salauddin Rasel, M. Salauddin, M. Toyabur Rahman, J. Y. Park, *Appl. Energy* **2019**, *256*, 113987; c) A. Zurbuchen, A. Haeberlin, L. Bereuter, A. Pfenniger, S. Bosshard, M. Kernen, P. Philipp Heinisch, J. Fuhrer, R. Vogel, *IEEE Trans. Biomed. Eng.* **2018**, *65*, 424.

[8] a) H. Yang, F. R. Fan, Y. Xi, W. Wu, *EcoMat* **2021**, *3*, e12093; b) W. He, W. Liu, J. Chen, Z. Wang, Y. Liu, X. Pu, H. Yang, Q. Tang, H. Yang, H. Guo, C. Hu, *Nat. Commun.* **2020**, *11*, 4277; c) Y. Liu, W. Liu, Z. Wang, W. He, Q. Tang, Y. Xi, X. Wang, H. Guo, C. Hu, *Nat. Commun.* **2020**, *11*, 1599; d) Y. Cao, Y. Yang, X. Qu, B. Shi, L. Xu, J. Xue, C. Wang, Y. Bai, Y. Gai, D. Luo, Z. Li, *Small Methods* **2022**, *6*, 2101529; e) Z. Wang, Z. Ruan, W. S. Ng, H. Li, Z. Tang, Z. Liu, Y. Wang, H. Hu, C. Zhi, *Small Methods* **2018**, *2*, 1800150.

[9] a) C. Zhang, W. Fan, S. Wang, Q. Wang, Y. Zhang, K. Dong, *ACS Appl. Electron. Mater.* **2021**, *3*, 2449; b) M. Zhang, T. Gao, J. Wang, J. Liao, Y. Qiu, Q. Yang, H. Xue, Z. Shi, Y. Zhao, Z. Xiong, L. Chen, *Nano Energy* **2015**, *13*, 298; c) S. A. Han, T. H. Kim, S. K. Kim, K. H. Lee, H. J. Park, J. H. Lee, S. W. Kim, *Adv. Mater.* **2018**, *30*, 1800342.

[10] a) Y. Yu, J. Nassar, C. Xu, J. Min, Y. Yang, A. Dai, R. Doshi, A. Huang, Y. Song, R. Gehlhar, A. Ames, W. Gao, *Sci. Rob.* **2020**, *5*, eaaz7946; b) M. Sun, Y. Gu, X. Pei, J. Wang, J. Liu, C. Ma, J. Bai, M. Zhou, *Nano Energy* **2021**, *86*, 106061; c) L.-L. Wang, H.-H. Shao, W.-J. Wang, J.-R. Zhang, J.-J. Zhu, *Nano Energy* **2018**, *44*, 95.

[11] a) M. M. , P. Rajagopalan, S. Xu, I. A. Palani, V. Singh, X. Wang, W. Wu, *Nanoscale* **2021**, *13*, 20615; b) H. Qiao, P. Zhao, O. Kwon, A. Sohn, F. Zhuo, D. M. Lee, C. Sun, D. Seol, D. Lee, S. W. Kim, Y. Kim, *Adv. Sci. (Weinh)* **2021**, *8*, 2101793; c) H. Ryu, H. M. Park, M. K. Kim, B. Kim, H. S. Myoung, T. Y. Kim, H. J. Yoon, S. S. Kwak, J. Kim, T. H. Hwang, E. K. Choi, S. W. Kim, *Nat. Commun.* **2021**, *12*, 4374; d) L. Gu, L. German, T. Li, J. Li, Y. Shao, Y. Long, J. Wang, X. Wang, *ACS Appl. Mater. Interfaces* **2021**, *13*, 5133.

[12] D. Guannan, W. Haifeng, G. Hui, G. Guobiao, *IEEE Trans. Appl. Supercond.* **2010**, *20*, 1883.

[13] a) C. Rodrigues, A. Gomes, A. Ghosh, A. Pereira, J. Ventura, *Nano Energy* **2019**, *62*, 660; b) M. S. Rasel, P. Maharjan, J. Y. Park, *Nano Energy* **2019**, *63*, 103816; c) P. Maharjan, T. Bhatta, C. Park, H. Cho, K. Shrestha, S. Lee, M. Salauddin, M. T. Rahman, S. M. S. Rana, J. Y. Park, *Nano Energy* **2021**, *88*, 106232; d) X. Guo, T. He, Z. Zhang, A. Luo, F. Wang, E. J. Ng, Y. Zhu, H. Liu, C. Lee, *ACS Nano* **2021**, *15*, 19054.

[14] a) N. Zhang, C. Qin, T. Feng, J. Li, Z. Yang, X. Sun, E. Liang, Y. Mao, X. Wang, *Nano Res.* **2020**, *13*, 1903; b) D. Jiang, H. Ouyang, B. Shi, Y. Zou, P. Tan, X. Qu, S. Chao, Y. Xi, C. Zhao, Y. Fan, Z. Li, *InfoMat* **2020**, *2*, 1191.

[15] a) H. Ouyang, Z. Liu, N. Li, B. Shi, Y. Zou, F. Xie, Y. Ma, Z. Li, H. Li, Q. Zheng, X. Qu, Y. Fan, Z. L. Wang, H. Zhang, Z. Li, *Nat. Commun.* **2019**, *10*, 1821; b) X. Qu, X. Ma, B. Shi, H. Li, L. Zheng, C. Wang, Z. Liu, Y. Fan, X. Chen, Z. Li, Z. L. Wang, *Adv. Funct. Mater.* **2020**, *31*,2006612.

[16] J. Li, T. A. Hacker, H. Wei, Y. Long, F. Yang, D. Ni, A. Rodgers, W. Cai, X. Wang, *Nano Energy* **2021**, *90*, 106507.

 © 2022 Wiley-VCH GmbH